Accumulation of alkyl-lysophosphatidylcholines in Niemann-Pick disease type C1

Sonali Mishra[1,‡] , Pamela Kell[1,‡], David Scherrer[1], Dennis J. Dietzen[2], Charles H. Vite[3], Elizabeth Berry-Kravis[4], Cristin Davidson[5], Stephanie M. Cologna[6] , Forbes D. Porter[5], Daniel S. Ory[7], and Xuntian Jiang[1*]

[1]Department of Medicine, and [2]Department of Pediatrics, Washington University School of Medicine, St. Louis, MO, USA; [3]Department of Clinical Studies and Advanced Medicine, University of Pennsylvania School of Veterinary Medicine, PA, USA; [4]Department of Pediatrics, Neurological Sciences and Anatomy and Cell Biology, Rush University Medical Center, Chicago, IL, USA; [5]Section on Molecular Dysmorphology, Eunice Kennedy Shriver National Institute of Child Health and Human Development, NIH, DHHS, Bethesda, MD, USA; [6]Department of Chemistry, University of Illinois Chicago, Chicago, IL, USA; and the [7]Arbor Biotechnologies, Cambridge, MA, USA

Abstract Lysosomal function is impaired in Niemann-Pick disease type C1 (NPC1), a rare and inherited neurodegenerative disorder, resulting in late endosomal/lysosomal accumulation of unesterified cholesterol. The precise pathogenic mechanism of NPC1 remains incompletely understood. In this study, we employed metabolomics to uncover secondary accumulated substances in NPC1. Our findings unveiled a substantial elevation in the levels of three alkyl-lysophosphatidylcholine [alkyl-LPC, also known as lyso-platelet activating factor (PAF)] species in NPC1 compared to controls across various tissues, including brain tissue from individuals with NPC1, liver, spleen, cerebrum, cerebellum, and brain stem from NPC1 mice, as well as in both brain and liver tissue from NPC1 cats. The three elevated alkyl-LPC species were as follows: LPC O-16:0, LPC O-18:1, and LPC O-18:0. However, the levels of PAF 16:0, PAF 18:1, and PAF 18:0 were not altered in NPC1. In the NPC1 feline model, the brain and liver alkyl-LPC levels were reduced following 2-hydroxypropyl-β-cyclo-dextrin (HPβCD) treatment, suggesting that alkyl-LPCs are secondary storage metabolites in NPC1 disease. Unexpectedly, cerebrospinal fluid (CSF) levels of LPC O-16:0 and LPC O-18:1 were decreased in individuals with NPC1 compared to age-appropriate comparison samples, and their levels were increased in 80% of participants 2 years after intrathecal HPβCD treatment. The fold increases in CSF LPC O-16:0 and LPC O-18:1 levels were more pronounced in responders compared to nonresponders. ⬛ This study identified alkyl-LPC species as secondary storage metabolites in NPC1 and indicates that LPC O-16:0 and LPC O-18:1, in particular, could serve as potential biomarkers for tracking treatment response in NPC1 patients.

Niemann-Pick disease type C (NPC) is a rare and inherited metabolic disorder characterized by progressive neurodegeneration (1). More than 95% of cases are caused by pathological variants in the *NPC1*, which encodes the NPC1 protein that plays a key role in egress of cholesterol from the lysosome (2). Individuals affected with NPC1 disease have impaired lysosomal function. Unesterified cholesterol accumulates within late endosomes/lysosomes and is accompanied by secondary storage of other lipids (3, 4), principally within liver, spleen, and brain tissues (5). This lipid storage results in disease of variable onset, including hepatosplenomegaly, prolonged neonatal cholestatic jaundice, and progressive neurological symptoms such as difficulty in coordinating movements, seizures, and cognitive decline (6, 7). In liver and spleen tissues, in addition to unesterified cholesterol (8, 9), there is accumulation of sphingomyelin (8–10), bis(monoacylglycerol) phosphate (8), glucosylceramide (8–10), lactosylceramide (8–11), gangliosides GM2 and GM3 (8–11), sphingosine (9–12), and sphinganine. The triacylglycerol level was found to increase in liver tissues (13). In brain tissue, cholesterol similarly accumulates in the late endosomal/lysosomal compartment of NPC1 neuronal cells, though its overall level is not increased (4). There are, however, significant secondary increases in glycosphingolipids, including gangliosides GM2 and GM3 (4, 9–11), lactosylceramide (4, 9–11), and glucosylceramide

---

(4, 9, 10). Sphingoid bases such as sphingosine (9–11) and sphinganine (9, 10) also show moderate elevations. In both liver and brain, there is a significant increase in N-palmitoyl-O-phosphocholineserine, which is the most abundant species among a class of lipids known as N-acyl-O-phosphocholineserines (14).

Three drugs that target different aspects of NPC1 disease pathology have completed phase 3 clinical trials (15). Miglustat, an inhibitor of glycosphingolipid synthesis, demonstrated efficacy in slowing neurological progression in NPC1 patients and received approval for use outside the United States (16–18). 2-Hydroxypropyl-β-cyclodextrin (HPβCD, adrabetadex) that releases cholesterol from lysosomes has shown significant therapeutic potential in NPC1 mouse and cat models (19). Arimoclomol is an inducer of HSP70 that prevents protein misfolding and has also been reported to have efficacy in the NPC1 mouse model (20). Both HPβCD (21) and arimoclomol (22) have shown reduction in disease progression and disease stabilization in clinical trials. However, neither has yet been approved for treatment of NPC1 by the US Food and Drug Administration despite very protracted development timelines. A major limitation for studying therapeutics in a rare, slowly progressive, highly heterogenous neurodegenerative disease, in which clinical outcomes are challenging to definitively prove over short time frames, is the lack of validated CNS biomarkers to monitor treatment efficacy (23).

Discovery of new secondary accumulation metabolites in NPC1 may identify novel treatment biomarkers, as well as offer new insights into the complex mechanisms involved in NPC1 pathology and open up potential therapeutic opportunities. In the present study, we used metabolomic profiling to discover such metabolites from the individuals with NPC1 as well as mouse and the feline models. The $Npc1^{-/-}$ mouse model, which arose from a spontaneous mutation, is widely accepted as a model for severe infantile cases (24). The cat model, characterized by a missense mutation in the NPC1 gene, exhibits clinical, neuropathological, and biochemical abnormalities akin to those observed in juvenile-onset patients (24). Utilizing samples from both patients and these two distinct animal models can help identify robust biomarkers for NPC1. Our findings reveal a significant elevation of alkyl-lysophosphatidylcholine [alkyl-LPC, also known as lyso-platelet activating activator (PAF)] species in brain tissue of individuals with NPC1, as well as in the liver, spleen, cerebrum, cerebellum, and brain stem of NPC1 mice, alongside elevated levels observed in both brain and liver tissue of NPC1 cats, in comparison to controls. Furthermore, in the feline model, the brain and liver alkyl-LPC levels were reduced following HPβCD intervention. These results implicate alkyl-LPC as a secondary storage metabolite that could prove useful as a therapeutic response biomarker. Further investigation into the role of alkyl-LPC in NPC1 disease pathology may also reveal novel therapeutic targets.

MATERIALS AND METHODS

Chemicals and reagents

Formic acid and CHAPS were obtained from VWR (West Chester, PA). All HPLC solvents (methanol, isopropanol, and acetonitrile) were HPLC grade and were purchased from EMD Chemicals (Gibbstown, NJ). Diisopropyl fluorophosphate (DIFP), ammonium acetate, d6-acetic anhydride, 4-dimethylaminopyridine, hydrochloride, and sodium hydroxide were from Sigma-Aldrich (St. Louis, MO). LPC O-16:0, LPC O-18:1, LPC O-18:0, d_4-LPC O-16:0, d_4-LPC O-18:0, PAF 16:0, PAF 18:1, PAF 18:0, d_4-PAF 16:0, and d_4-PAF 18:0 were provided by Cayman Chemical (Ann Arbor, MI). Milli-Q ultrapure water was prepared in-house with a Milli-Q Integral Water Purification System (Billerica, MA).

Ethics

Human studies adhered to the principles of the Declaration of Helsinki, as well as to Title 45, US Code of Federal Regulations, Part 46, Protection of Human Subjects. Informed consent was obtained from the participants or their guardians. Approval for clinical protocols was granted by the Institutional Review Boards of NICHD/ National Institutes of Health (NIH), Rush University Medical Center, and St. Louis Children's Hospital. All the clinical samples were deidentified, and the analysis of deidentified human samples was approved by the Human Studies Committee at Washington University. NPC1 cats were raised in the animal colony of the School of Veterinary Medicine at the University of Pennsylvania under NIH and US Department of Agriculture guidelines for the care and use of animals in research. Mice were maintained in a breeding colony at NIH. Experimental procedures were approved by the University of Pennsylvania and NIH Animal Studies Committees and were conducted in accordance with the US Department of Agriculture Animal Welfare Act and the Public Health Service Policy for the Humane Care and Use of Laboratory Animals.

Human brain, plasma, and cerebrospinal fluid samples

Human brain samples were obtained from the NIH NeuroBioBank, Rockville, MD. The postmortem brain tissues including cerebellum, dorsolateral prefrontal cortex, and hippocampus were collected from three individuals with NPC1 and three healthy subjects who died from accidents. All plasma samples were collected in ethylenediamine tetraacetic acid dipotassium (K$_2$EDTA) containing tubes. The NPC1 plasma samples were collected from a natural history study of NPC disease conducted at the NIH Clinical Center. Normal plasma samples were obtained from anonymized residual samples at St. Louis Children's Hospital. The Phase two-thirds sham-controlled trial of biweekly intrathecal (IT) doses of 900 mg of HPβCD followed by an open-label extension with 400–900 mg and an expanded access program using biweekly IT doses of 200–1200 mg of HPβCD were performed at Rush University Medical Center and the NIH Clinical Center. The detailed protocol was described in recent papers (25, 26). Cerebrospinal fluid (CSF) (1 ml) from treated NPC1 study participants was collected via lumbar puncture into polypropylene tubes preloaded with 20 mg of CHAPS. Age-appropriate CSF samples were collected into polypropylene tubes from pediatric patients with other clinical indications at St. Louis Children's Hospital, and the final CHAPS concentration was 2% (w/v).

The demographic characteristics of participants are listed in Table 1.

Mouse tissue samples

Heterozygous $Npc1^{+/-}$ mice (BALB/c Nctr-$Npc1^{m1N}$/J strain) were intercrossed to obtain control ($Npc1^{+/+}$) and mutant ($Npc1^{-/-}$) littermates. For tissue collection, $Npc1^{-/-}$ and $Npc1^{+/+}$ mice were euthanized at 7 weeks of age using a rising concentration of carbon dioxide. The blood was collected in K_2EDTA tube with DIFP and centrifuged at 4°C and 1500 g for 10 min, and K_2EDTA plasma with DIFP (1 mM) was transferred into a separated tube. The liver, spleen, cerebrum, cerebellum, and brain stem were collected, flash frozen, and stored at −80°C until use.

Cat tissue samples

NPC1 cats received intracisternal (IC) HPβCD (120 mg total) every 14 days or combination of 1000 mg/kg subcutaneous (SC) HPβCD every 7 days and 120 mg IC HPβCD every 14 days beginning at 3 weeks of age, and brain and liver tissues were collected as described previously (11).

Nomenclature of alkyl-LPC and PAF species

The alkyl-LPC and PAF were described as LPC O-x:y and PAF x:y, respectively, where x and y are the number of carbon atoms and the total number of double bonds of alkyl group, respectively (27).

Metabolomic profiling of brain samples from NPC1 patients and control subjects for biomarker discovery

The preparation of brain homogenates, extraction of metabolites, and liquid chromatography-high resolution mass spectrometry (LC-HRMS) methods for biomarker discovery and confirmation are described in Supplementary Information.

Structural identification of alkyl-LPC

The LC-high resolution tandem mass spectrometry (HRMS2) methods for $[M+H]^+$ and $[M+CH_3CO_2]^-$ ions of LPC O-16:0, LPC O-18:1, and LPC O-18:0, hydrogen/deuterium (H/D) exchange experiment, treatment with acid and base, and acetylation with d_6-acetic anhydride are described in Supplementary Information.

Analysis of alkyl-LPC in biomarker verification

Analysis of alkyl-LPC in human brain, human plasma, human CSF, mouse plasma, mouse liver, mouse spleen, mouse cerebrum, mouse cerebellum, mouse brain stem, cat brain, and cat liver for biomarker verification is described in Supplementary Information.

Analysis of PAF

Analysis of PAF is described in Supplementary Information.

STATISTICS

The data normality was checked with Shapiro-Wilk test. Normally distributed data were analyzed using t test or ANOVA. Nonnormally distributed data were analyzed using Wilcoxon signed-rank test or Mann-Whitney test or Kruskal-Wallis test.

RESULTS

Discovery of NPC1 central nervous system biomarkers

We obtained dorsolateral prefrontal cortex, hippocampus, and cerebellum from NPC1 patients and age- and sex-matched controls. To assess the differences in metabolomic profiling between NPC1 and control tissues, we performed an untargeted metabolomics analysis using LC-HRMS on an Exploris-120 orbitrap mass spectrometer. Full mass scans in both positive and negative ion modes were employed to detect metabolites, and metabolites were separated under both acidic and neutral mobile phase conditions of reversed phase liquid chromatography and hydrophilic interaction liquid chromatography (total 8 LC-HRMS runs). We found that the sensitivities of low abundant metabolites detected with mass range of 100–2000 were significantly lower than those with narrow mass range, because automatic gain control was used to prevent the overfilling of C-trap and Orbitrap core cell, and the detection of low abundant ions is adversely affected by the total number of trapped ions (28). To enhance the detection sensitivity, the mass range of 100–2000 was divided into 19 segments with segment width of 100 and 1 m/z small overlaps in adjacent segments so that the total trapped ions were reduced. The narrower mass segment increased the detectable ions but at the expense of increase of LC-HRMS runs to 19 per LC condition or ion mode. Pooling extracts of individual NPC1 and control samples to give two samples were

TABLE 1. Demographic characteristics of human subjects

Cohort	Sample Type	Patient Type	NPC1	Control
Biomarker discovery with metabolomics	Brain	Age (range, median; mean ± SD)	2 - 17, 13; 10 ± 7.5	2 - 17, 11; 10.7 ± 7.7
		Male/Female (n/n)	2/1	2/1
Biomarker evaluation	Plasma	Age (range, median; mean ± SD)	1 - 17, 8; 8 ± 6.3	1 - 18, 7; 8.7 ± 7.4
		Male/Female (n/n)	4/3	4/3
	CSF	Age when trial started (range, median; mean ± SD)	6 - 31, 28; 20.2 ± 13	6 - 21, 16.5; 16 ± 4.5
		Male/Female (n/n)	4/1	7/3

CSF, cerebrospinal fluid; NPC1, Niemann-Pick disease type C1.

employed to improve throughput in discovery bio-analysis by reducing the number of samples analyzed. A total of 152 LC-HRMS runs were utilized to analyze two pooled samples in triplicate in the discovery step. We selected for study only metabolites that showed large difference between NPC1 and control; features with at least 5-fold difference were chosen and reanalyzed in individual brain samples to confirm the variation in NPC1. Our workflow strategy is shown in **Fig. 1**. Potential biomarkers were submitted for structural identification.

Three unknown features with m/z 482, 508, and 510 detected in positive ion mode, and all the LC conditions were elevated >5-fold in all three regions of NPC1 brains, and they appeared as m/z 540, 566, and 568 ions in negative ion mode and neutral LC conditions in which ammonium acetate was used as buffer. The data

from neutral reversed phase liquid chromatography in positive and negative ion modes are presented in supplemental Fig. S1. Experimentally determined accurate masses, retention times, and predicted formulas are given in Table 2.

Identification of structures of potential NPC1 biomarkers as alkyl-LPCs

From the predicted formulas, we deduced that m/z 482/540, m/z 508/566, and m/z 510/568 ions were $[M+H]^+/[M+CH_3CO_2]^-$ ions of three metabolites. The degrees of unsaturation of both m/z 482 and 510 features are 0, indicating that they contain no double bond or ring. The m/z 508 feature contains a double bond.

To gain insight into the structures of three metabolites, we optimized the LC conditions to separate them from interferences with same nominal mass and obtained clean HRMS2 spectra. In addition to product ions resulting from loss of water (**1**), fragmentation of m/z 482, 508, and 510 features also generated protonated trimethylamine (**2**), vinyltrimethylammonium (**3**), coline (**4**), protonated ethylene phosphate (**5**), and protonated phosphocholine (**6**), indicating that they contain a phosphocholine group (Table 3). The higher-energy collisional dissociation spectra of m/z 540, 566, 568 features show product ions $[M+CH_3CO_2-CH_3CO_2CH_3]^-$ (**7**), $[M-phosphocholine]^-$ (**8**), $[M-phosphocholine-H_2O]^-$ (**9**), 2-(dimethylamino)ethyl (oxiran-2-ylmethyl) phosphate (**10**), $[phosphocholine-CH_3]^-$ (**11**), phosphate (**12**), metaphosphate (**13**), and acetate (**14**), confirming that phosphocholine group presents in these metabolites (Table 4).

The H/D exchange experiment detected only one exchangeable hydrogen atoms in m/z 482, 508, and 510 features (supplemental Fig. S2), suggesting that these features contain a single hydroxyl group. The presence of the hydroxyl group was confirmed by formation of d_3-acetates after treatment with d_6-acetic anhydride (supplemental Fig. S3). Jones oxidation of m/z 482, 508, and 510 features produced only ketone derivatives detected as $[M+H]^+$ at m/z 480.3450 (calculated mass: 480.3449), 506.3605 (calculated mass: 506.3605), and 508.3761 (calculated mass: 508.3762) (supplemental Fig. S4), respectively, indicating the presence of secondary hydroxyl groups in these metabolites. The m/z 482, 508, and 510 features were not decomposed under acidic and basic condition, suggesting that they did not contain acidic and basic liable groups, such as vinyl ether, epoxide, and carboxylic esters.

Exclusive of the phosphocholine and secondary hydroxyl group, the remaining moieties of m/z 482, 508, and 510 features are $C_{19}H_{38}O$, $C_{21}H_{40}O$, and $C_{21}H_{42}O$, respectively. These moieties consist of two alkyl groups connected by an ether bond. As no further structural information was available, we utilized the molecular formulas to search the Scifinder database (https://scifinder-n.cas.org) for compounds with phosphocholine, secondary hydroxyl group, and two alkyl groups

NPC1 human brain 1   **Control human brain 1**
NPC1 human brain 2   **Control human brain 2**
....
NPC1 human brain n   **Control human brain n**

Extraction and pooling extracts

Pooled NPC1 human brain extract   **Pooled control human brain extract**

Acidic RPLC
Neutral RPLC
Acidic HILIC
Neutral HILIC

Positive HRMS
m/z 100 - 200
m/z 200 - 300
m/z 300 - 400
....
m/z 1900 - 2000

Negative HRMS
m/z 100 - 200
m/z 200 - 300
m/z 300 - 400
....
m/z 1900 - 2000

Features with > 5-fold difference between NPC1 and control

Analysis of identified features in individual NPC1 and control samples and confirmation of differences between NPC1 and control

Structural identification of biomarkers
1. HRMS2
2. H/D exchange experiemnt
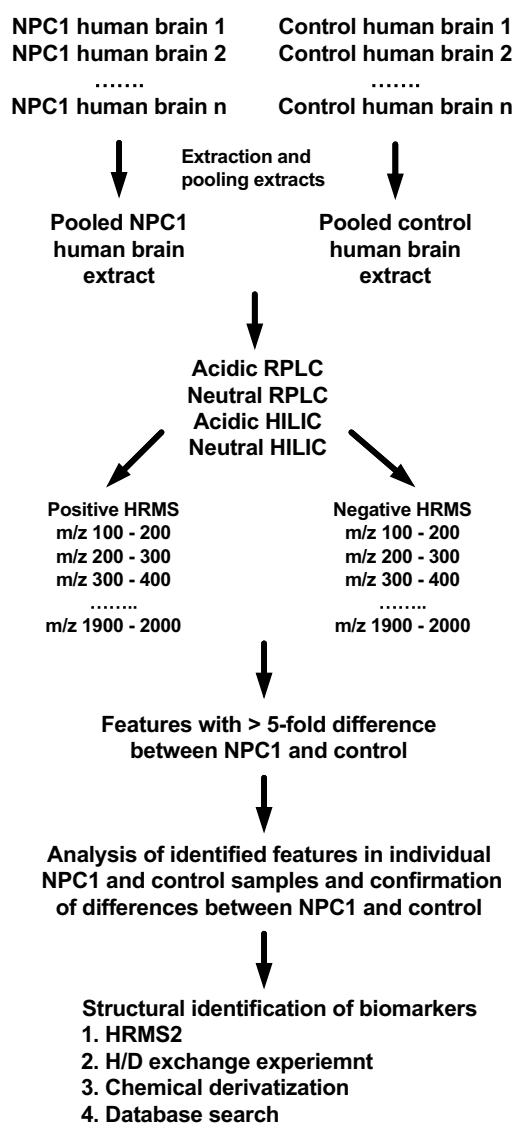**3. Chemical derivatization**
4. Database search

Fig. 1. Strategy of biomarker discovery with untargeted metabolomics. HILIC, hydrophilic interaction liquid chromatography; RPLC, reversed phase liquid chromatography.

TABLE 2. Ion mode, LC conditions, accurate masses of pseudo-molecular ions, and retention times of LPC O-16:0, LPC O-18:1, and LPC O-18:0 in the biomarker discovery

Metabolite	LC Condition	Ion Mode	Detected m/z	Pseudo-molecular Ion, Formula, Theoretical m/z	Deviation (ppm)	Retention Time (min)
LPC O-16:0	Acidic RPLC	Positive	482.3613	$[M+H]^+$	1.66	9.4
	Neutral RPLC		482.3606	$C_{24}H_{53}NO_6P$ m/z 482.3605	0.21	9.4
	Acidic HILIC		482.3614		1.87	8.5
	Neutral HILIC		482.3606		0.21	8.3
LPC O-18:1	Acidic RPLC		508.3772	$[M+H]^+$	1.97	9.6
	Neutral RPLC		508.3756	$C_{26}H_{55}NO_6P$ m/z 508.3762	−1.18	9.5
	Acidic HILIC		508.3776		2.75	8.5
	Neutral HILIC		508.3765		0.59	8.3
LPC O-18:0	Acidic RPLC		510.393	$[M+H]^+$	2.35	10
	Neutral RPLC		510.3912	$C_{26}H_{57}NO_6P$ m/z 510.3918	−1.18	9.9
	Acidic HILIC		510.3932		2.74	8.5
	Neutral HILIC		510.3919		0.20	8.3
LPC O-16:0	Neutral RPLC	Negative	540.368	$[M+CH_3CO_2]^-$ $C_{26}H_{55}NO_8P$ m/z 540.3665	2.78	9.4
	Neutral HILIC		540.3688		4.26	8.3
LPC O-18:1	Neutral RPLC		566.3843	$[M+CH_3CO_2]^-$ $C_{28}H_{57}NO_8P$ m/z 566.3822	3.71	9.5
	Neutral HILIC		566.3844		3.88	8.3
LPC O-18:0	Neutral RPLC		568.3999	$[M+CH_3CO_2]^-$ $C_{28}H_{59}NO_8P$ m/z 568.3984	3.69	9.9
	Neutral HILIC		568.3996		3.17	8.3

HILIC, hydrophilic interaction liquid chromatography; LC, liquid chromatography; LPC, lysophosphatidylcholine; RPLC, reversed phase liquid chromatography.

connected by an ether bond. Consequently, we identified the following matches: LPC O-16:0 for m/z 482, LPC O-18:1 for m/z 508, and LPC O-18:0 for m/z 510. Comparison of LC-HRMS2 spectra of synthetic and endogenous compounds confirmed the structural identification (**Fig. 2** and supplemental Fig. S5).

Alkyl-LPCs are NPC1 biomarkers

After identifying the structures of alkyl-LPCs, we used commercial standard compounds and deuterated internal standards to develop a highly sensitive and reproducible liquid chromatography-tandem mass spectrometry (LC-MS/MS) method for alkyl-LPCs on a

6500 QTRAP + mass spectrometer and confirmed the elevation of alkyl-LPCs in NPC1 patient brains on this different analytical platform (**Fig. 3**). Next, we tested if the alkyl-LPC markers were present in NPC1 mouse and cat models. LPC O-16:0, LPC O-18:1, and LPC O-18:0 levels exhibited significant elevation in the liver, spleen, cerebrum, cerebellum, and brain stem of NPC1 mice (**Fig. 4**A–C), as well as in the brain and liver of untreated NPC1 cats (**Fig. 5**A, B), in comparison to those in normal animals. Unexpectedly, these alkyl-LPCs were significantly reduced in NPC1 mouse plasma, though the fold changes were less than 2.2-fold.

TABLE 3. Product ions from fragmentation of features m/z 482, 508, and 510 in positive mode
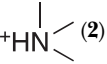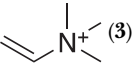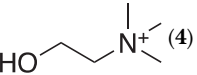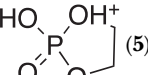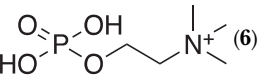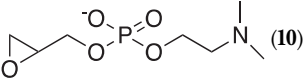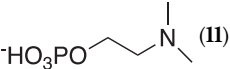
Product Ion	Feature m/z 482 Formula Detected Mass (Calculated Mass) Deviation (ppm)	Feature m/z 508 Formula Detected Mass (Calculated Mass) Deviation (ppm)	Feature m/z 510 Formula Detected Mass (Calculated Mass) Deviation (ppm)
$[M+H-H_2O]^+$ (1)	$C_{24}H_{51}NO_5P^+$ 464.3504 (464.3499) 1.08	$C_{26}H_{53}NO_5P^+$ 490.3659 (490.3656) 0.61	$C_{26}H_{55}NO_5P^+$ 492.3820 (492.3812) 1.62
^+HN (2)	$C_3H_{10}N^+$ 60.0808 (60.0808) 0	$C_3H_{10}N^+$ 60.0808 (60.0808) 0	$C_3H_{10}N^+$ 60.0808 (60.0808) 0
N^+ (3)	$C_5H_{12}N^+$ 86.0965 (86.0964) 1.16	$C_5H_{12}N^+$ 86.0964 (86.0964) 0	$C_5H_{12}N^+$ 86.0965 (86.0964) 1.16
HO—N^+ (4)	$C_5H_{14}NO^+$ 104.1071 (104.1070) 0.96	$C_5H_{14}NO^+$ 104.1070 (104.1070) 0	$C_5H_{14}NO^+$ 104.1071 (104.1070) 0.96
HO—P (5)	$C_2H_6O_4P^+$ 124.9999 (124.9998) 0.8	$C_2H_6O_4P^+$ 124.9999 (124.9999) 0	$C_2H_6O_4P^+$ 124.9999 (124.9998) 0.8
P—N^+ (6)	$C_5H_{15}NO_4P^+$ 184.0734 (184.0733) 0.54	$C_5H_{15}NO_4P^+$ 184.0734 (184.0733) 0.54	$C_5H_{15}NO_4P^+$ 184.0735 (184.0733) 1.09

TABLE 4. Product ions from fragmentation of features m/z 540, 566, and 568 in negative mode

Product Ion	Feature m/z 540 Formula Detected Mass (Calculated mass) Deviation (ppm)	Feature m/z 566 Formula Detected Mass (Calculated mass) Deviation (ppm)	Feature m/z 568 Formula Detected Mass (Calculated mass) Deviation (ppm)
$[M+CH_3CO_2-CH_3CO_2CH_3]^-$ (7)	$C_{23}H_{49}NO_6P^-$ 466.3316 (466.3303) 2.79	$C_{25}H_{51}NO_6P$ 492.3471 (492.3460) 2.23	$C_{25}H_{53}NO_6P^-$ 494.3631 (494.3616) 3.03
$[M\text{-phosphocholine}]^-$ (8)	$C_{19}H_{40}O_6P^-$ 395.2580 (395.2568) 3.04	$C_{21}H_{42}NO_6P^-$ 421.2737 (421.2725) 2.85	$C_{21}H_{44}NO_6P^-$ 423.2897 (423.2881) 3.78
$[M\text{-phosphocholine-}H_2O]^-$ (9)	$C_{19}H_{38}O_5P^-$ 377.2475 (377.2462) 3.45	$C_{21}H_{40}NO_5P^-$ 403.2631 (403.2619) 3.31	$C_{21}H_{42}NO_5P^-$ 405.2791 (405.2775) 3.95
(10)	$C_7H_{15}NO_5P^-$ 224.0696 (224.0693) 1.34	$C_7H_{15}NO_5P^-$ 224.0695 (224.0693) 0.89	$C_7H_{15}NO_5P^-$ 224.0697 (224.0693) 1.79
(11)	$C_4H_{11}NO_4P^-$ 168.0431 (168.0435) −2.38	$C_4H_{11}NO_4P^-$ 168.0431 (168.0435) −2.38	$C_4H_{11}NO_4P^-$ 168.0432 (168.0435) −1.79
$H_2PO_4^-$ (12)	$H_2PO_4^-$ 96.9695 (96.9696) −1.03	$H_2PO_4^-$ 96.9695 (96.9696) −1.03	$H_2PO_4^-$ 96.9696 (96.9696) 0
PO_3^- (13)	PO_3^- 78.9590 (78.9591) −1.27	PO_3^- 78.9590 (78.9591) −1.27	PO_3^- 78.9590 (78.9591) −1.27
$CH_3CO_2^-$ (14)	$CH_3CO_2^-$ 59.0140 (59.0140) 0	$CH_3CO_2^-$ 59.0140 (59.0140) 0	$CH_3CO_2^-$ 59.0139 (59.0140) 0

Alkyl-LPCs respond to 2-hydroxypropyl-β-cyclodextrin treatment

In cats receiving IC HPβCD (100 mg/kg) every 14 days beginning at 3 weeks of age, the LPC O-16:0, LPC O-18:1, and LPC O-18:0 were reduced by 47%, 54%, and 53%, respectively. Similarly, the LPC O-16:0, LPC O-18:1, and LPC O-18:0 were reduced by 56%, 66%, and 54% in the cats receiving combination of 1000 mg/kg SC HPβCD every 7 days and 120 mg IC HPβCD every 14 days beginning at 3 weeks of age, respectively (Fig. 5A). Due to small sample size, the change of LPC O-18:1 in the brains of cats treated with IC HPβCD versus untreated cats did not reach statistical significance ($P = 0.0513$). The LPC O-16:0, LPC O-18:1, and LPC O-18:0 were also significantly elevated in livers of untreated NPC1 cats. In the livers from IC HPβCD-treated cats, LPC O-16:0, LPC O-18:1, and LPC O-18:0 levels were increased by 25%, 31%, 23%, respectively, compared to untreated cats. A 53%, 58%, and 43% reduction of liver LPC O-16:0, LPC O-18:1, and LPC O-18:0, respectively, was seen in NPC1 cats receiving SC and IC HPβCD treatment (Fig. 5B). These results suggest that IC HPβCD dose was insufficient to reduce the alkyl-LPCs in liver, which agrees with unchanged storage of cholesterol and sphingomyelin in IC HPβCD-treated cat livers (11).

Alkyl-LPCs in human plasma and CSF

To explore the potential of application of alkyl-LPCs to serve as biomarkers for clinical use, we measured these metabolites in plasma and CSF samples from NPC1 and control individuals. The NPC1 plasma samples were collected from a natural history study. The CSF samples were collected from 10 control subjects and five NPC1 patients enrolled in an IT HPβCD treatment protocol at visit 2 after a single dose of HPβCD, and at years 1, 2, and 3 of treatment. None of the alkyl-LPCs was significantly changed in plasmas from untreated NPC1 patients in natural history study compared to controls (Fig. 6A–C). Among the NPC1 subjects, there were two responders (NPC-11 and NPC-38) and three nonresponders (NPC-04, NPC-10, and NPC-15) to HPβCD treatment, who showed < 0.5/year and > 0.5/year increases on the total NPC neurological disease severity score, respectively. These samples provided an opportunity to investigate the long-term effect of HPβCD treatment on alkyl-LPCs. Similar to NPC1 mouse plasma, the LPC O-16:0 and LPC O-18:1 levels in NPC1 CSF collected at visit 2 were significantly lower than controls, while LPC O-18:0 showed no significant difference between NPC1 and control. LPC O-16:0 and LPC O-18:1 in CSF collected at visit 2 did not differentiate responders from nonresponders. After 2 years of IT cyclodextrin treatment, most of patients show increase of CSF LPC O-16:0 (Fig. 6D) and LPC O-18:1 (Fig. 6E) except for NPC-04 compared to visit 2, and the responders show a larger fold increase than nonresponders (Fig. 6G, H). The CSF LPC O-18:0 was also increased after 2 years cyclodextrin treatment, although the fold change did not provide a clear separation of responders from non-responder (Fig. 6I). Data so far are limited to a small number of treated patients, but CSF LPC O-16:0 and LPC O-18:1 may have potential as predictive biomarkers to differentiate responders from nonresponders.
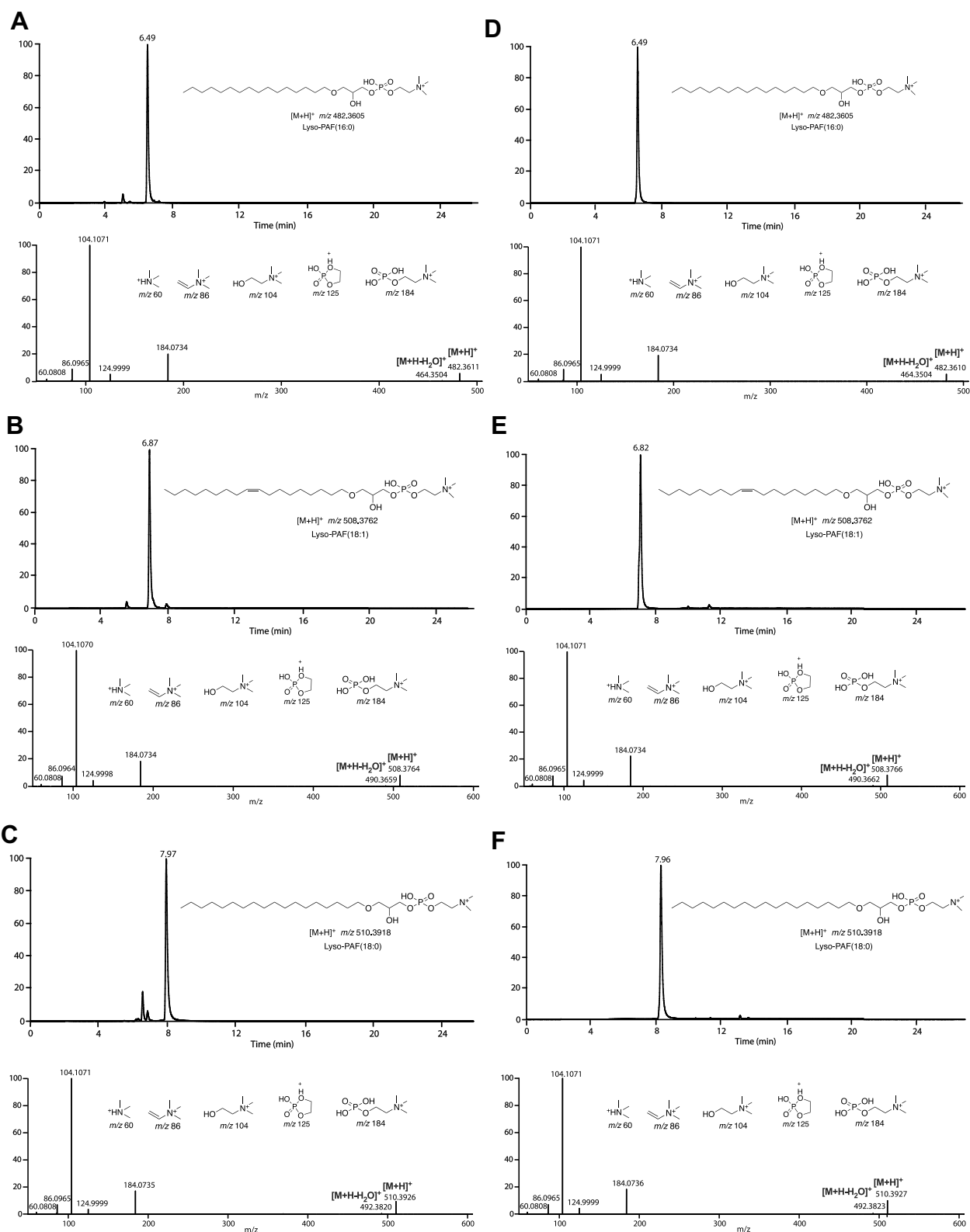
Fig. 2. Comparison of endogenous and synthetic alkyl-LPC. The LC-HRMS2 of [M+H]$^+$ ions of endogenous LPC O-16:0 (A), endogenous LPC O-18:1 (B), and endogenous LPC O-18:0 (C), synthetic LPC O-16:0 (D), synthetic LPC O-18:1 (E), and synthetic LPC O-18:0 (F). Proposed structures of product ions are given.

PAFs are unchanged in NPC1

As alkyl-LPCs are precursors and metabolites of PAFs, we also analyzed PAFs in human brain, plasma, and CSF, as well as in cat brain and liver, and in mouse liver, spleen, cerebrum, cerebellum, and brain stem. Quantification of PAF 16:0 was challenging due to their low abundances and the presence of large isomeric LPC 18:0, which produced same product ions from [M+H]$^+$
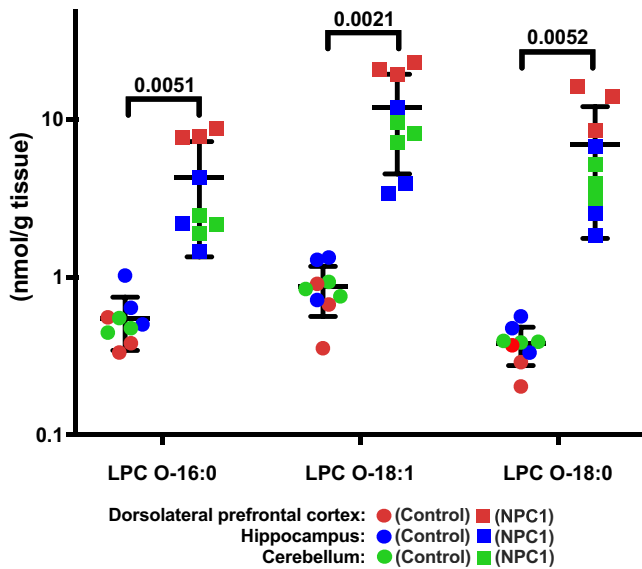
Fig. 3. Alkyl-LPCs in human brain measured in the biomarker verification. LPC O-16:0, LPC O-18:1, and LPC O-18:0 in dorsolateral prefrontal cortex (red), hippocampus (blue), cerebellum (green) from NPC1 patients (square) and control subjects (circle). The data are presented as mean ± standard deviation. Comparison of NPC1 and control was performed with t test with Welch's correction. P-values < 0.05 are given above brackets.

and $[M+CH_3CO_2]^-$ precursor ions. PAF is rapidly converted to alkyl-LPC by PAF acetylhydrolase (29–31), with a reported half-life of 4–14 min in human serum (29). To address this, we developed a LC-MS/MS method in which PAF and LPC were separated at baseline. The tissue homogenates were prepared in methanol-water (7:3) with PAF acetylhydrolase inhibitor DIFP (1 mM) and citric acid (20 mM), pH 5, to prevent PAF degradation (30). PAFs were undetectable in all the archived human brain, plasma, and CSF samples, as well as cat tissues used in this study. Freshly collected mouse plasma and tissues were employed for PAF analysis, and K_2EDTA mouse plasma was supplemented with DIFP (1 mM). Surprisingly, PAF level remained unchanged in NPC1 disease (supplemental Fig. S6A–C).

DISCUSSION

NPC1 is a rare lipid storage disorder characterized by, in addition to endolysosomal unesterified cholesterol accumulation, alterations in lysosomal calcium homeostasis and signaling pathways, mitochondrial dysfunction, increased inflammation, oxidative stress, and decreased autophagy flux, ultimately leading to neuronal degeneration (32, 33). Advances in our understanding of the molecular pathogenesis of NPC1 disease have led to development of stabilizing treatment approaches that aim to reduce the accumulation of gangliosides in the brain through the use of miglustat and to decrease lysosomal cholesterol level by employing HPβCD (15, 34). Despite this progress, there are no FDA-approved disease-modulating therapies for
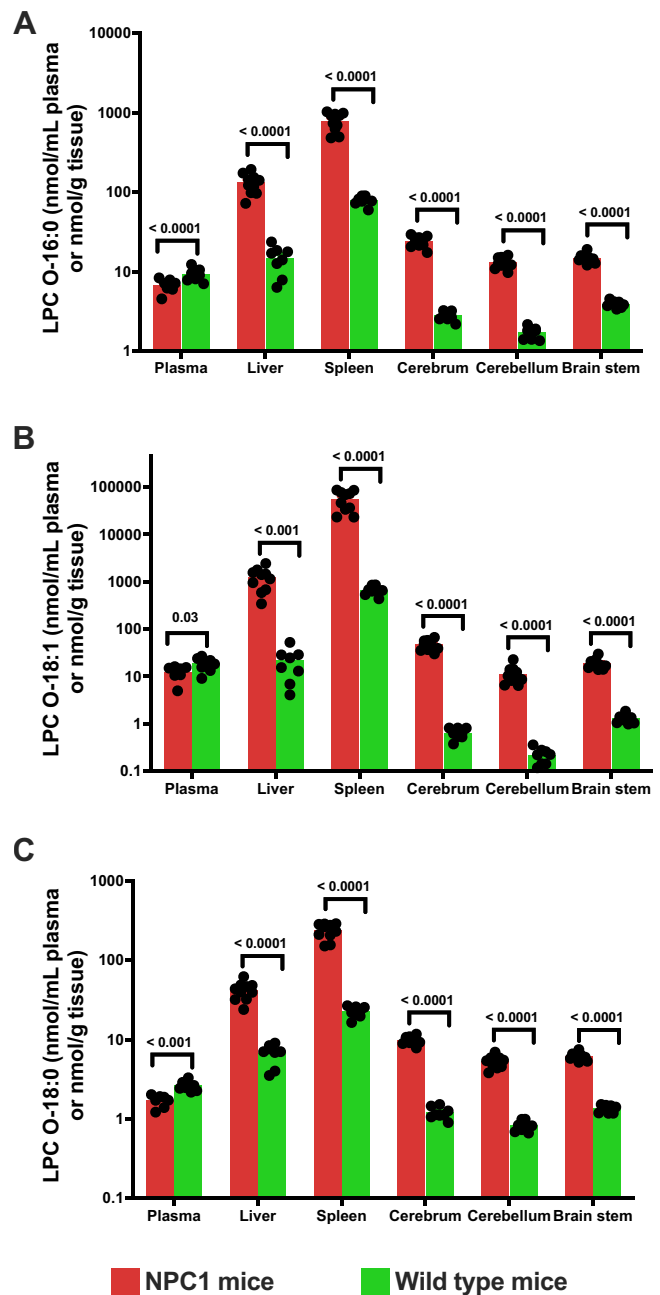

Fig. 4. Alkyl-LPCs in mouse tissues. LPC O-16:0 (A), LPC O-18:1 (B), and LPC O-18:0 (C) in plasma, liver, spleen, cerebrum, cerebellum, and brain stem collected from NPC1 mice (n = 9) and wild-type mice (n = 6). Three NPC1 plasma samples were excluded from the analysis due to severe hemolysis of the blood. Data are presented as mean ± standard error of the mean. Data comparison for alkyl-LPCs was performed with t test. P-values < 0.05 are given above brackets.

NPC1 disease. A major limitation has been the lack of established biomarkers to monitor response to treatment. In the present study, we addressed this unmet need through use of metabolomic profiling of patient samples, a strategy that previously led to discovery of oxysterols, bile acids, and N-palmitoyl-O-phosphocholineserine—metabolites that have transformed NPC1 diagnostics (35) and have raised the potential for newborn screening (36).
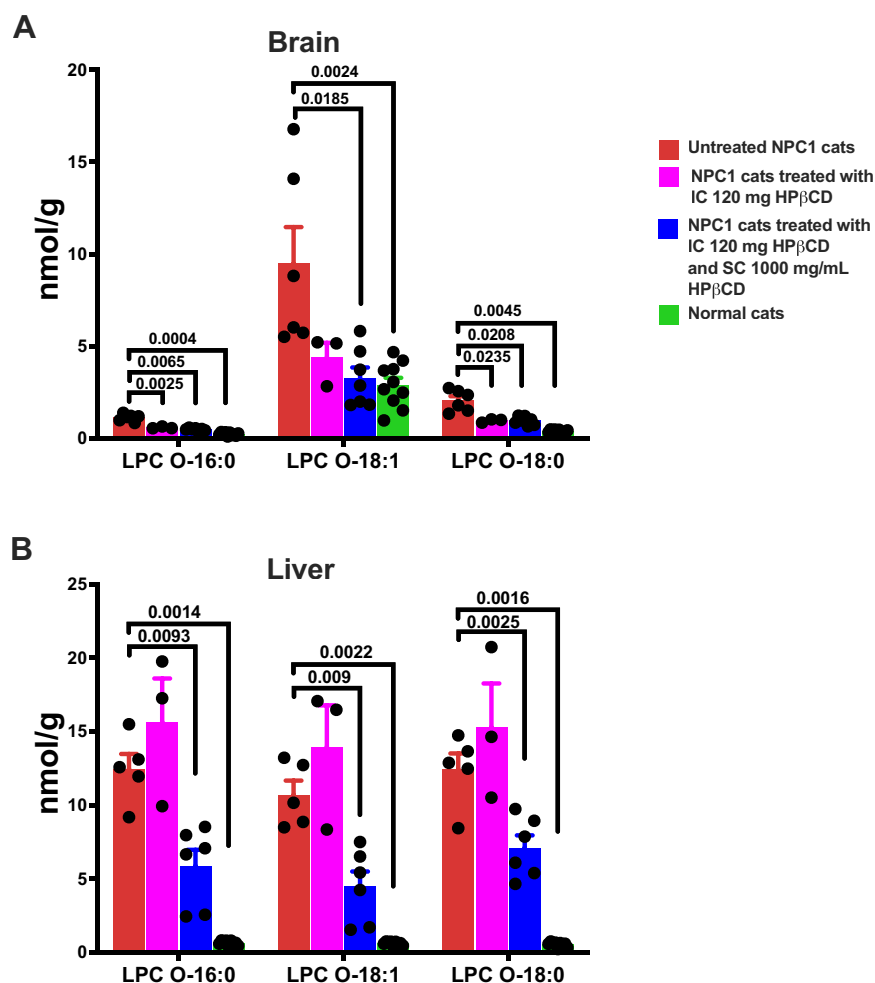
Fig. 5. Alkyl-LPCs in cat brain and liver. (A) LPC O-16:0, LPC O-18:1, and LPC O-18:0 in brains of untreated NPC1 cats (n = 6), NPC1 cats treated with IC 120 mg HPβCD (n = 3), NPC1 cats treated with IC 120 mg HPβCD and SC 1000 mg/kg HPβCD (n = 7), and normal cats (n = 10). Data are presented as mean ± standard error of the mean. Data comparison for LPC O-16:0 and LPC O-18:0 was performed with Brown-Forsythe and Welch ANOVA test with Dunnett's T3 multiple comparisons test as post hoc test. Data comparison for LPC O-18:1 was performed with Kruskal-Wallis test with Dunn's multiple comparisons test as post hoc test. *P*-values < 0.05 are given above brackets. (B) LPC O-16:0, LPC O-18:1, and LPC O-18:0 in livers of untreated NPC1 cats (n = 5), NPC1 cats treated with IC 120 mg HPβCD (n = 3), NPC1 cats treated with IC 120 mg HPβCD and SC 1000 mg/kg HPβCD (n = 6), and normal cats (n = 9). Data are normalized to mean of untreated NPC1 cats and presented as mean ± standard error of the mean. Data comparison for LPC O-16:0, LPC O-18:1, and LPC O-18:0 was performed with Brown-Forsythe and Welch ANOVA test with Dunnett's T3 multiple comparisons test as post hoc test. *P*-values < 0.05 are given above brackets.

In the present study, untargeted metabolomic profiling identified LPC O-16:0, LPC O-18:1, and LPC O-18:0 as secondary storage metabolites in NPC1 tissues. The structures of these metabolites were determined using HRMS2, H/D exchange experiment, and chemical derivatizations; further confirmation was obtained through LC-MS/MS comparison with standard compounds. Significantly higher levels of alkyl-LPCs were observed in the brains of NPC1 patients, as well as in the brains and livers of NPC1 cats, and liver, spleen, cerebrum, cerebellum, and brain stem of NPC1 mice. Treatment with IC and SC HPβCD reduced alkyl-LPCs in the NPC1 cat brain and liver, respectively, suggesting that the clearance of alkyl-LPCs was a result of restoration of lysosomal homeostasis by HPβCD.

The exact mechanism underlying the elevation of alkyl-LPCs in NPC1 remains unknown. Alkyl-LPC synthesis involves phospholipase A2 hydrolysis of membrane alkyl-phosphatidylcholine, followed by acetylation to generate PAF (37). Increase of amyloid-β42 was found in NPC1 (38–41), and amyloid-β42 was reported to activate cytosolic phospholipase A2 and cause accumulation of alkyl-LPCs and PAF in Alzheimer disease (42, 43). PAF is a proinflammatory messenger and a mediator of neurotoxicity implicated in neurodegeneration (44, 45). However, the PAFs in liver, spleen, cerebrum, cerebellum, and brain stem of NPC1 mice remained unchanged.

The potential of alkyl-LPCs in human plasma and CSF as a biomarker to monitor treatment efficacy was also explored in the study. Although the alkyl-LPC levels
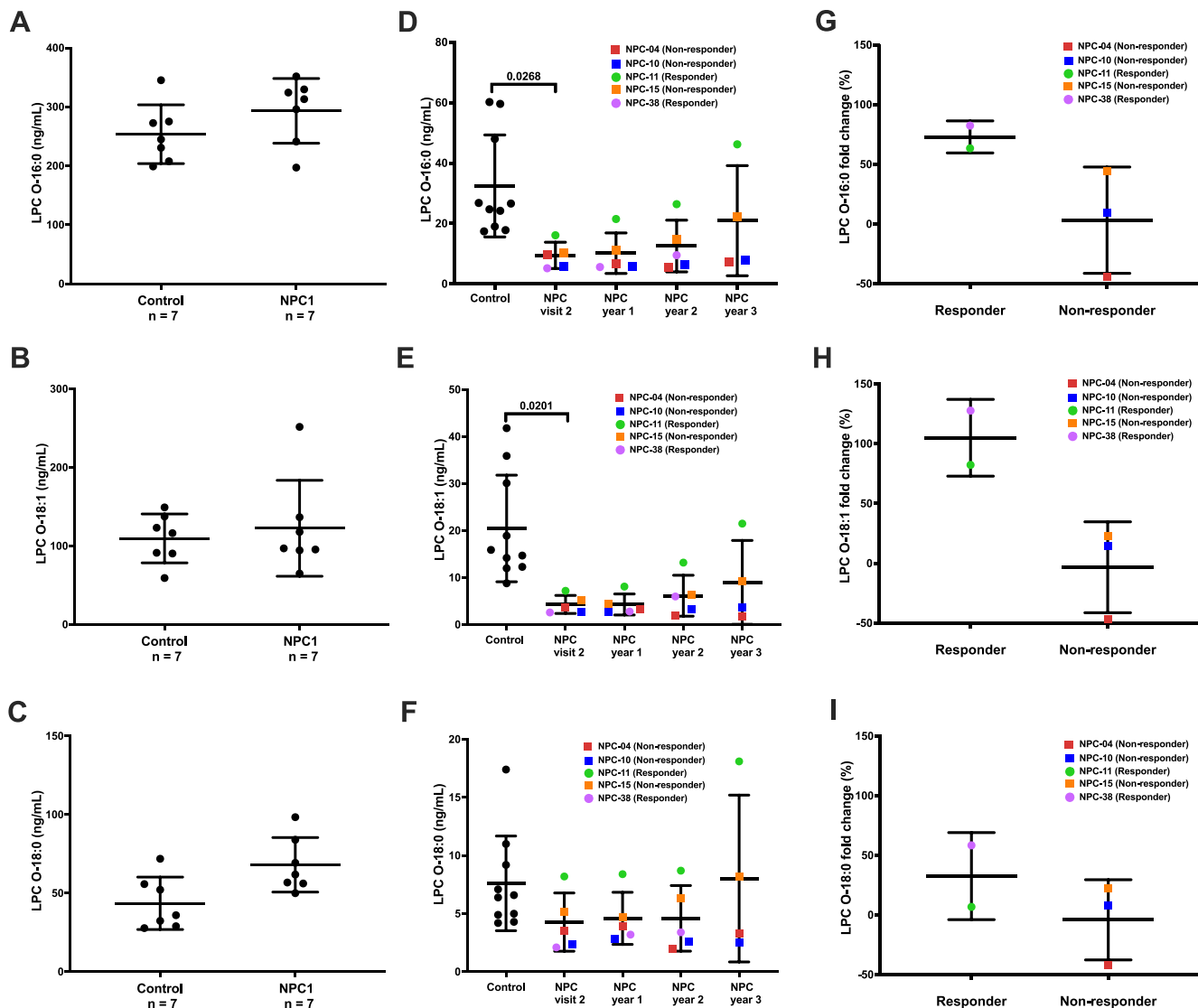
Fig. 6. Alkyl-LPCs in human plasma and CSF. LPC O-16:0 (A), LPC O-18:1 (B), and LPC O-18:0 (C) in plasma from NPC1 patients (n = 7) and control subjects (n = 7). Data are presented as mean ± standard deviation. t test with Welch's correction was used to compare NPC1 and controls. LPC O-16:0 (D), LPC O-18:1 (E), and LPC O-18:0 (F) in CSF from NPC1 patients (n = 5) and control subjects (n = 10). Data are presented as median ± interquartile. Data comparison was performed with Kruskal-Wallis test with Dunn's multiple comparisons test as post hoc test. P-values < 0.05 are given above brackets. Fold change of LPC O-16:0 (G), LPC O-18:1 (H), and LPC O-18:0 (I) at year 2 compared to visit 2. Data are presented as median ± interquartile. Statistical analysis was not performed for the fold change of LPC O-16:0 and LPC O-18:1 due to small sample size.

remained unchanged in NPC1 plasma, there were notable alterations observed in NPC1 CSF. Specifically, both LPC O-16:0 and LPC O-18:1 levels were significantly reduced in the CSF of individuals with NPC1. Interestingly, the alkyl-LPCs were observed to accumulate in NPC1 mouse peripheral tissues but to decrease in plasma. The reason for accumulation of LPC O-16:0 and LPC O-18:1 in brain but reduction in CSF from individuals with NPC1 is unclear, although may suggest cellular accumulation is associated with a block of normal release from CNS cells. Intriguingly, these metabolites were increased in 80% of participants 2 years post IT HPβCD treatment. The fold increases in CSF LPC O-16:0 and LPC O-18:1 levels were more pronounced in responders compared to nonresponders,

indicating that LPC O-16:0 and LPC O-18:1 may serve as potential pharmacodynamic biomarkers for monitoring treatment response in the CNS of NPC1 patients who show positive responses to this therapeutic intervention. The responsiveness of alkyl-LPC levels in the CSF may also be indicative of a favorable treatment outcome, showing that the treatment is effectively targeting the underlying disease mechanisms in the CNS. Further research utilizing more samples and validation studies are warranted to harness the full potential of alkyl-LPC as a clinical tool for monitoring treatment response in this challenging disorder.

In conclusion, we used metabolomics to identify alkyl-LPCs as secondary storage metabolite in NPC1 disease. Alkyl-LPC species may serve as potential

markers for NPC1 pathogenesis, a target for therapeutic intervention and for treatment-response monitoring. Our findings underscore the complexity of NPC1 and the need for further research to fully explore the potential of alkyl-LPCs as a clinical tool in managing this challenging disorder.

Data availability

The data described in this article are presented in the figures or supplemental materials. JLR

Author contributions

S. M. and P. K. validation; S. M. and P. K. formal analysis; S. M. and P. K. investigation; S. M., P. K., C. D., and X. J. data curation; P. K., D. S., and C. D. investigation; D. J. D., C. H. V., E. B.-K., and F. D. P. resources; D. J. D., C. H. V., E. B.-K., C.D., S. M. C., F. D. P., and D. S. O. writing–review & editing; D. J. D., C. H. V., E. B.-K., S. M. C., F. D. P., D. S. O., and X. J. supervision; D. J. D., C. H. V., E. B.-K., S. M. C., F. D. P., D. S. O., and X. J. project administration; C. H. V., E. B.-K., S. M. C., F. D. P., D. S. O., and X. J. funding acquisition; E. B.-K., S. M. C., F. D. P., D. S. O., and X. J. conceptualization; S. M. C., X. J., and D. S. O. methodology; D. S. O. and X. J. visualization; X. J. writing–original draft.

Author ORCIDs

Sonali Mishra https://orcid.org/0000-0003-3464-4894
Stephanie M. Cologna https://orcid.org/0000-0002-3541-3361
Xuntian Jiang https://orcid.org/0000-0001-9048-7294

Abbreviations

CSF, cerebrospinal fluid; DIFP, diisopropyl fluorophosphate; H/D, hydrogen/deuterium exchange; HILIC, hydrophilic interaction liquid chromatography; HPβCD, 2-hydroxypropyl-β-cyclodextrin; IC, intracisternal; IT, intrathecal; LC, liquid chromatography; HRMS, high resolution mass spectrometry; HRMS2, high-resolution tandem mass spectrometry; LC-MS/MS, liquid chromatography-tandem mass spectrometry; LPC, lysophosphatidylcholine; NPC, Niemann-Pick disease type C; PAF, platelet activating activator; RPLC, reversed phase liquid chromatography; SC, subcutaneous.

REFERENCES

1. Vanier, M. T. (2010) Niemann-Pick disease type C. *Orphanet J. Rare Dis.* **5**, 16
2. Runz, H., Dolle, D., Schlitter, A. M., and Zschocke, J. (2008) NPC-db, a Niemann-Pick type C disease gene variation database. *Hum. Mutat.* **29**, 345–350
3. Platt, F. M. (2023) The expanding boundaries of sphingolipid lysosomal storage diseases; insights from Niemann-Pick disease type C. *Biochem. Soc. Trans.* **51**, 1777–1787
4. Vanier, M. T. (1999) Lipid changes in Niemann-Pick disease type C brain: personal experience and review of the literature. *Neurochem. Res.* **24**, 481–489
5. Vanier, M. T. (2015) Complex lipid trafficking in Niemann-Pick disease type C. *J. Inherit. Metab. Dis.* **38**, 187–199
6. Bonnot, O., Gama, C. S., Mengel, E., Pineda, M., Vanier, M. T., Watson, L., *et al.* (2019) Psychiatric and neurological symptoms in patients with Niemann-pick disease type C (NP-C): findings from the international NPC registry. *World J. Biol. Psychiatry.* **20**, 310–319
7. Bolton, S. C., Soran, V., Marfa, M. P., Imrie, J., Gissen, P., Jahnova, H., *et al.* (2022) Clinical disease characteristics of patients with Niemann-pick disease type C: findings from the international Niemann-pick disease registry (INPDR). *Orphanet J. Rare Dis.* **17**, 51
8. Vanier, M. T. (1983) Biochemical studies in Niemann-Pick disease. I. Major sphingolipids of liver and spleen. *Biochim. Biophys. Acta.* **750**, 178–184
9. Praggastis, M., Tortelli, B., Zhang, J., Fujiwara, H., Sidhu, R., Chacko, A., *et al.* (2015) A murine Niemann-Pick C1 I1061T knock-in model recapitulates the pathological features of the most prevalent human disease allele. *J. Neurosci.* **35**, 8091–8106
10. Fan, M., Sidhu, R., Fujiwara, H., Tortelli, B., Zhang, J., Davidson, C., *et al.* (2013) Identification of Niemann-Pick C1 disease biomarkers through sphingolipid profiling. *J. Lipid Res.* **54**, 2800–2814
11. Vite, C. H., Bagel, J. H., Swain, G. P., Prociuk, M., Sikora, T. U., Stein, V. M., *et al.* (2015) Intracisternal cyclodextrin prevents cerebellar dysfunction and Purkinje cell death in feline Niemann-Pick type C1 disease. *Sci. Transl. Med.* **7**, 276ra226
12. Rodriguez-Lafrasse, C., Rousson, R., Pentchev, P. G., Louisot, P., and Vanier, M. T. (1994) Free sphingoid bases in tissues from patients with type C Niemann-Pick disease and other lysosomal storage disorders. *Biochim. Biophys. Acta.* **1226**, 138–144
13. Garver, W. S., Jelinek, D., Oyarzo, J. N., Flynn, J., Zuckerman, M., Krishnan, K., *et al.* (2007) Characterization of liver disease and lipid metabolism in the Niemann-Pick C1 mouse. *J. Cell Biochem.* **101**, 498–516
14. Sidhu, R., Mondjinou, Y., Qian, M., Song, H., Kumar, A. B., Hong, X., *et al.* (2019) N-acyl-O-phosphocholineserines: structures of a

novel class of lipids that are biomarkers for Niemann-Pick C1 disease. *J. Lipid Res.* **60**, 1410–1424

15. Sitarska, D., Tylki-Szymanska, A., and Lugowska, A. (2021) Treatment trials in Niemann-Pick type C disease. *Metab. Brain Dis.* **36**, 2215–2221

16. Patterson, M. C., Garver, W. S., Giugliani, R., Imrie, J., Jahnova, H., Meaney, F. J., *et al.* (2020) Long-term survival outcomes of patients with Niemann-Pick disease type C receiving miglustat treatment: a large retrospective observational study. *J. Inherit. Metab. Dis.* **43**, 1060–1069

17. Patterson, M. C., Mengel, E., Vanier, M. T., Moneuse, P., Rosenberg, D., and Pineda, M. (2020) Treatment outcomes following continuous miglustat therapy in patients with Niemann-Pick disease Type C: a final report of the NPC Registry. *Orphanet J. Rare Dis.* **15**, 104

18. Patterson, M. C., Vecchio, D., Prady, H., Abel, L., and Wraith, J. E. (2007) Miglustat for treatment of Niemann-Pick C disease: a randomised controlled study. *Lancet Neurol.* **6**, 765–772

19. Braga, S. S. (2023) Molecular mind games: the medicinal action of cyclodextrins in neurodegenerative diseases. *Biomolecules.* **13**, 666

20. Kirkegaard, T., Gray, J., Priestman, D. A., Wallom, K. L., Atkins, J., Olsen, O. D., *et al.* (2016) Heat shock protein-based therapy as a potential candidate for treating the sphingolipidoses. *Sci. Transl. Med.* **8**, 355ra118

21. Ory, D. S., Ottinger, E. A., Farhat, N. Y., King, K. A., Jiang, X., Weissfeld, L., *et al.* (2017) Intrathecal 2-hydroxypropyl-beta-cyclodextrin decreases neurological disease progression in Niemann-Pick disease, type C1: a non-randomised, open-label, phase 1-2 trial. *Lancet.* **390**, 1758–1768

22. Mengel, E., Patterson, M. C., Da Riol, R. M., Del Toro, M., Deodato, F., Gautschi, M., *et al.* (2021) Efficacy and safety of arimoclomol in Niemann-Pick disease type C: results from a double-blind, randomised, placebo-controlled, multinational phase 2/3 trial of a novel treatment. *J. Inherit. Metab. Dis.* **44**, 1463–1480

23. Berry-Kravis, E. (2021) Niemann-Pick disease, type C: diagnosis, management and disease-targeted therapies in development. *Semin. Pediatr. Neurol.* **37**, 100879

24. Pallottini, V., and Pfrieger, F. W. (2020) Understanding and treating Niemann-pick type C disease: models matter. *Int. J. Mol. Sci.* **21**, 8979

25. Berry-Kravis, E., Chin, J., Hoffmann, A., Winston, A., Stoner, R., LaGorio, L., *et al.* (2018) Long-term treatment of Niemann-pick type C1 disease with intrathecal 2-Hydroxypropyl-beta-Cyclodextrin. *Pediatr. Neurol.* **80**, 24–34

26. Albert, O. K., Friedmann, K., Jaeger, R., and Berry-Kravis, E. (2023) Low risk profile of long-term repeated lumbar puncture for intrathecal delivery of 2-hydroxypropyl-beta-cyclodextrin in patients with Niemann-pick type C. *Pediatr. Neurol.* **144**, 99–103

27. Liebisch, G., Fahy, E., Aoki, J., Dennis, E. A., Durand, T., Ejsing, C. S., *et al.* (2020) Update on LIPID MAPS classification, nomenclature, and shorthand notation for MS-derived lipid structures. *J. Lipid Res.* **61**, 1539–1555

28. Wang, C. F., and Li, L. (2022) Segment scan mass spectral acquisition for increasing the metabolite detectability in chemical isotope labeling liquid chromatography-mass spectrometry metabolome analysis. *Anal. Chem.* **94**, 11650–11658

29. Vadas, P., Gold, M., Perelman, B., Liss, G. M., Lack, G., Blyth, T., *et al.* (2008) Platelet-activating factor, PAF acetylhydrolase, and severe anaphylaxis. *N. Engl. J. Med.* **358**, 28–35

30. Hattori, M., Arai, H., and Inoue, K. (1993) Purification and characterization of bovine brain platelet-activating factor acetylhydrolase. *J. Biol. Chem.* **268**, 18748–18753

31. Owen, J. S., Thomas, M. J., and Wykle, R. L. (2007) Platelet-activating factor. *Methods Enzymol.* **434**, 105–116

32. Breiden, B., and Sandhoff, K. (2020) Mechanism of secondary ganglioside and lipid accumulation in lysosomal disease. *Int. J. Mol. Sci.* **21**, 2566

33. Yanez, M. J., Marin, T., Balboa, E., Klein, A. D., Alvarez, A. R., and Zanlungo, S. (2020) Finding pathogenic commonalities between Niemann-Pick type C and other lysosomal storage disorders: opportunities for shared therapeutic interventions. *Biochim. Biophys. Acta Mol. Basis Dis.* **1866**, 165875

34. Santos-Lozano, A., Villamandos Garcia, D., Sanchis-Gomar, F., Fiuza-Luces, C., Pareja-Galeano, H., Garatachea, N., *et al.* (2015) Niemann-Pick disease treatment: a systematic review of clinical trials. *Ann. Transl. Med.* **3**, 360

35. Jiang, X., and Ory, D. S. (2021) Advancing diagnosis and treatment of Niemann-pick C disease through biomarker discovery. *Explor Neuroprotective Ther.* **1**, 146–158

36. Jiang, X., Sidhu, R., Mydock-McGrane, L., Hsu, F. F., Covey, D. F., Scherrer, D. E., *et al.* (2016) Development of a bile acid-based newborn screen for Niemann-Pick disease type C. *Sci. Transl. Med.* **8**, 337ra363

37. Kita, Y., Ohto, T., Uozumi, N., and Shimizu, T. (2006) Biochemical properties and pathophysiological roles of cytosolic phospholipase A2s. *Biochim. Biophys. Acta.* **1761**, 1317–1322

38. Yamazaki, T., Chang, T. Y., Haass, C., and Ihara, Y. (2001) Accumulation and aggregation of amyloid beta-protein in late endosomes of Niemann-pick type C cells. *J. Biol. Chem.* **276**, 4454–4460

39. Mattsson, N., Zetterberg, H., Bianconi, S., Yanjanin, N. M., Fu, R., Mansson, J. E., *et al.* (2011) Gamma-secretase-dependent amyloid-beta is increased in Niemann-Pick type C: a cross-sectional study. *Neurology.* **76**, 366–372

40. Runz, H., Rietdorf, J., Tomic, I., de Bernard, M., Beyreuther, K., Pepperkok, R., *et al.* (2002) Inhibition of intracellular cholesterol transport alters presenilin localization and amyloid precursor protein processing in neuronal cells. *J. Neurosci.* **22**, 1679–1689

41. Jin, L. W., Shie, F. S., Maezawa, I., Vincent, I., and Bird, T. (2004) Intracellular accumulation of amyloidogenic fragments of amyloid-beta precursor protein in neurons with Niemann-Pick type C defects is associated with endosomal abnormalities. *Am. J. Pathol.* **164**, 975–985

42. Kriem, B., Sponne, I., Fifre, A., Malaplate-Armand, C., Lozac'h-Pillot, K., Koziel, V., *et al.* (2005) Cytosolic phospholipase A2 mediates neuronal apoptosis induced by soluble oligomers of the amyloid-beta peptide. *FASEB J.* **19**, 85–87

43. Sanchez-Mejia, R. O., Newman, J. W., Toh, S., Yu, G. Q., Zhou, Y., Halabisky, B., *et al.* (2008) Phospholipase A2 reduction ameliorates cognitive deficits in a mouse model of Alzheimer's disease. *Nat. Neurosci.* **11**, 1311–1318

44. Goracci, G., Balestrieri, M. L., and Nardicchi, V. (2009) Metabolism and functions of platelet activating factor (PAF) in the nervous tissue. In *Handbook of neurochemistry and molecular neurobiology.* Springer Science, Boston, MA, 311–352

45. Dorninger, F., Forss-Petter, S., Wimmer, I., and Berger, J. (2020) Plasmalogens, platelet-activating factor and beyond - ether lipids in signaling and neurodegeneration. *Neurobiol. Dis.* **145**, 105061

ASBMB